Titania-functionalized diatom frustules as photocatalyst for indoor air purification

Title: Titania-functionalized diatom frustules as photocatalyst for indoor air purification

Authors: Judith Ouwehand, Erik Van Eynde, Els De Canck, Silvia Lenaerts, An Verberckmoes, Pascal Van Der Voort

PII: S0926-3373(17)31212-2
DOI: https://doi.org/10.1016/j.apcatb.2017.12.063
Reference: APCATB 16298

To appear in: *Applied Catalysis B: Environmental*

Received date: 30-10-2017
Revised date: 20-12-2017
Accepted date: 23-12-2017

Please cite this article as: Judith Ouwehand, Erik Van Eynde, Els De Canck, Silvia Lenaerts, An Verberckmoes, Pascal Van Der Voort, Titania-functionalized diatom frustules as photocatalyst for indoor air purification, Applied Catalysis B, Environmental https://doi.org/10.1016/j.apcatb.2017.12.063

Titania-functionalized diatom frustules as photocatalyst for indoor air purification

Judith Ouwehand[a], Erik Van Eynde[b], Els De Canck[a], Silvia Lenaerts[b], An Verberckmoes[c], Pascal Van Der Voort[a*]

[a] Department of Chemistry, Ghent University, Krijgslaan 281-S3, 9000 Ghent, Belgium.
[b] Department of Bioscience Engineering, University of Antwerp, Groenenborgerlaan 171, 2020 Antwerp, Belgium.
[c] Department of Materials, Textiles and Chemical Engineering, Ghent University, Valentin Vaerwyckweg 1, 9000 Ghent, Belgium.
*Corresponding author: pascal.vandervoort@ugent.be

Graphical abstract

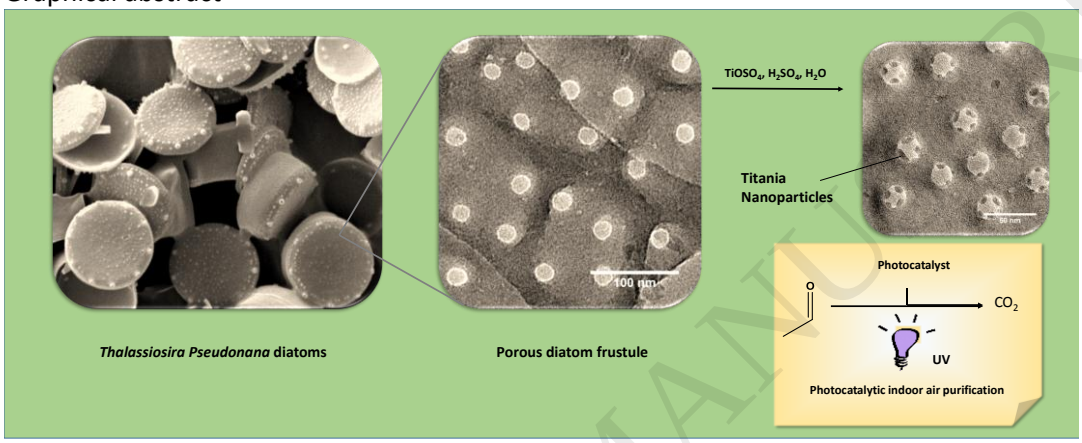

Highlights

- Silica frustules were extracted from diatoms, with a high surface area of 115 m²/g.
- The frustules were functionalized with titania nanoparticles.
- These materials are active in the photocatalytic degradation of acetaldehyde.
- The materials perform well in humid air for 48 hours of continuous reaction.

Abstract

Diatom frustules were extracted from the species *Thalassiosira pseudonana* and functionalized with titania to be used as photocatalysts in the abatement of acetaldehyde. The synthetic procedure is water-based and environmentally friendly. The synthesis parameters were optimized to give the highest possible photocatalytic activity. The optimized material, visualized with TEM and STEM-EDX, shows the TiO_2 nanoparticles grafted inside the frustule pores, as well as on the silica surface. The titania particles, stabilized by the frustules, are 2.5 times more active than the P25 benchmark material. The photocatalyst is then tested in conditions of elevated relative humidity, to simulate indoor air. The catalytic activity only shows a minor decrease at 50% relative humidity, which is a better result than for the P25 benchmark. When tested over an extended period of time, the photocatalyst only shows a minor decrease in activity.

Keywords

Titania, diatom frustule, photocatalysis, acetaldehyde degradation

1. Introduction

Diatoms are single-celled algae which produce intricate amorphous silica structures as a protective shell. [1] These frustules consist of well-defined silica structures, unique to each species. The large scale production of diatoms is expected to increase in coming years, in view of their potential in the production of biofuels. [2] In fact, research towards the production of these alternative fuels from renewable sources has become very important in recent years. Diatoms contain 15 to 80 percent (by weight of dry biomass) of oil, [3] depending on the species, which makes them a viable competitor for crops as a biofuel source. Like plants, diatoms metabolize carbon via photosynthesis, which makes the process of harvesting the biofuel CO_2-neutral. They also present certain practical advantages, such as a high growth rate and the very little space required to grow them. Besides organic compounds, diatoms also contain amorphous silica, in the form of frustules. Therefore, frustules are expected to be an important side product of the biofuel production process. [4]

Furthermore, diatom frustules present certain structural differences compared to commercial or synthetic porous silica sources. While commercial silica gel has a high specific surface area, the pores are not well defined as they are formed randomly during the production process. [5] Uniform pore size distributions can be obtained in synthetic silicas, such as zeolites or MCM and SBA-type mesoporous materials. However, in these cases, the pore sizes and morphologies which can be obtained are limited. Diatom frustules on the other hand are biologically synthesized by the organism, resulting in very well-defined structures. While many different diatom species exist with a wide variety of pore sizes and shapes, the morphology of the frustules is uniform for each species. [6, 7] They combine the advantages of a wide scope of pore morphologies with a well-defined pore structure.

TiO_2/SiO_2 hybrid materials are widely studied, [8, 9] because the photocatalytic activity of the crystalline titania phase can be improved by deposition on a silica carrier material. This is due to the stabilization of the titania nanoparticles on the silica surface, which limits the nanoparticle growth and inhibits aggregation of the nanoparticles. [10] Mostly, TiO_2/SiO_2 composites are formed by the sol-gel synthesis of a combination of Si and Ti precursors. However, it is also possible to post-functionalize a pre-formed silica material such as SBA-15 [11-14] or silica gel. [15-17] Diatom frustules have also been functionalized, using different titania precursors, such as titanium(IV)isopropoxide, [18-20] titanium(IV)butoxide, [21-23] titanium(IV)chloride [24] and titanyl sulfate. [25] In this work, we use the non-toxic and water soluble titania precursor titanyl sulfate in a straightforward impregnation procedure. This makes the synthetic process environmentally friendly, as the alternative titanium alkoxides and titanium chloride salts are much more toxic and often require processing in organic solvents. Additionally, in this procedure, all the titania is deposited onto the frustules, so no titanium-containing waste is produced.

The BET surface area of diatom frustules varies greatly, depending on the diatom species, ranging from below 10 m^2/g to above 150 m^2/g. [26] In this work, we selected the *Thalassiosira pseudonana* species, because of its high surface area and its straightforward and fast cultivation. The synthesis of the photocatalyst was optimized by varying the Ti/Si ratio and the calcination temperature and duration.

The titania-coated frustules were applied in the photocatalytic degradation of gaseous acetaldehyde. Titania is known to oxidatively decompose volatile organic compounds (VOCs) under UV irradiation due to its semiconductor properties. The UV light excites an electron from the valence band to the conduction band, creating an electron-hole pair. These charge carriers can form several active radical species by interacting with oxygen or water molecules in the environment. These $OH\cdot$ and $O_2^{-}\cdot$ species can oxidize VOCs and completely decompose them, resulting in the formation of CO_2 and H_2O. [8]

Acetaldehyde was chosen as a benchmark VOC, because of its presence in typical polluted indoor air, such as in office buildings. [27] It has previously been shown that titania photocatalysts can break down mixtures of several carbonyl compounds, [17] as well as aromatics and aliphatics [28]. Therefore, titania-silica photocatalysts have great potential for real applications in indoor air purification systems. In order to further investigate the behaviour of our material in more relevant conditions, the photocatalytic behaviour was also studied as a function of the relative humidity and for a prolonged period of time.

2. Experimental

2.1 Procedure for frustule extraction

Thalassiosira pseudonana was isolated from the North Sea at Oostende (Belgium) and cultivated on large scale in 10 m^3 raceway ponds at the facilities of TomAlgae (Nevele, Belgium). At the end of the cultivation the algae were harvested and upconcentration of the biomass into an algae paste was performed using the Evodos T25 spiral plate separator equipment. The obtained diatom paste has a dry weight of approximately 5wt% and was stored in a freezer at -20°C up to use. The extraction of the frustules from the biomass started with 500 ml of the frozen diatom paste, which was allowed to thaw at room temperature for 6 hours. The resulting liquid was divided over several centrifuge tubes and washed by adding distilled water, followed by centrifugation at 2000 rpm during 10 minutes. The decanted washing water was tested for the presence of chlorides by adding a few drops of a 0.1M solution of $AgNO_3$ (Sigma Aldrich, <99%). The washing cycle was repeated until no white AgCl precipitation was formed. The washed algae were collected, diluted to a total volume of 1L with distilled water, and then 350 mL HCl (37%, Carl Roth) was added. This mixture was stirred overnight and then repeatedly washed by adding distilled water, followed by centrifugation and decantation. The washing cycles were repeated until the washing water was at pH 5-6. The resulting green paste was dried at 60°C for 3 hours, followed by calcination in air at 550°C (heating rate 60°C/h) for 6 hours. The resulting white silica material was crushed with a pestle and mortar to form a fine powder. This procedure yielded up to 7 g of silica.

2.2 Titania functionalization procedure

An amount of 0.32 g Titanium(IV) oxysulfate - sulfuric acid hydrate (Sigma Aldrich, also referred to as titanyl sulfate in this work) was added to 4 mL of distilled water and heated at 65°C until the product fully dissolved. After cooling down to room temperature, 0.4 g of frustules were added and the mixture was stirred at 500 rpm for 2 hours. The mixture was then heated to 55°C and stirred at 150 rpm until all the liquid was evaporated. The resulting solid was calcined in air at 550°C (heating rate 60°C/h) for 3 hours. This procedure yields approximately 20 m% titania on the silica support. The same method was performed using different calcination temperatures and durations (see Table 2) and with different precursor ratios (see Table 3).

2.3 Photocatalytic abatement of acetaldehyde

The photocatalytic performance of the prepared diatom-TiO_2 samples towards the degradation of gas phase acetaldehyde is tested using the photocatalytic test setup described in detail by Tytgat et al. [29] All samples were first suspended in water (20 mg powder + 2 mL water) and stirred ultrasonically for 30 min. On two silicon wafers (2.5 x 1.5 cm^2), 500 µL of the suspension was drop casted. The slides were left to dry in an oven at 70°C for 2h. As a reference, the photocatalytic activity of Aerolyst P25 titania nanoparticles (Evonik) is also determined. The P25 sample is pretreated in the same manner.

The details of the continuous photocatalytic setup are described in the supporting information. Each photodegradation experiment consisted of 4 subsequent phases: (1) 10 min gas flow (400 cm^3 min^{-1}) in bypass, (2) 15 min gas flow through the dark reactor in order to achieve adsorption/desorption equilibrium, (3) 20 min gas flow through the reactor under UV-illumination and (4) 5 min air flow (flush phase) through the dark reactor. Before the experiment starts the samples are pretreated with UV for 30 minutes. For the extended activity measurement, phase (3) is extended to 47.3 hours. During these different phases detection of acetaldehyde and carbon dioxide in the gas effluent was carried out using a Nicolet™ 380 FTIR spectrometer (Thermo Fisher Scientific) with ZnSe windows and a 2 m heated gas cell. Spectra were recorded in a range of 4000 – 400 cm^{-1}. The used ν_{C2H4O} and ν_{CO2} stretch band positions of acetaldehyde and CO_2 are located at 2728 and 2360 cm^{-1} respectively. The peak heights at these wavenumbers are correlated with concentrations using a calibration curve.

2.4 Characterization methods

XRF measurements were performed on a NEX CG from Rigaku. CoO and TiO_2 were measured at different ratios to obtain a linear calibration curve. Photocatalyst samples were weighed and mixed with a known amount of CoO to determine the loading of TiO_2. For the trace element analysis, the quantification was directly performed by the apparatus.

XRD was performed with an ARL X'TRA apparatus (Thermo Scientific). Average crystallite sizes were determined using the Scherrer equation on the (101) reflection of the anatase phase by using: $d = \frac{0.9\lambda}{(\beta - b)cos\theta}$, where d is the crystallite size, λ is the X-ray wavelength, β is the peak width (FWHM), b is the instrumental peak width (determined by measuring LaB_6 crystals) and θ is the diffraction angle.

Elemental analysis was performed with a Thermo Flash 2000 Thermal Analyzer (Thermo Scientific). Nitrogen-sorption measurements were performed with a TriStar 3000 analyzer (Micromeritics). TEM and STEM-EDX measurements were performed on a JEOL JEM 2200-FS. SEM measurements were performed on a JEOL JSM 7600F FEG.

All measurements were performed after drying of the sample under vacuum at 120°C.

3. Results and discussion

3.1 Extraction and characterization of frustules

Diatom frustules were extracted from a sample containing a cultivation of *Thalassiosira pseudonana* in its salt water medium. After an initial washing procedure to remove the majority of the salts, an acid treatment was used to remove any remaining carbonates and partially digest the organic matter. After washing away the acid, calcination in air at 550°C was used to completely free the frustules of organic components. The purity of the resulting frustules was assessed by a quantitative analysis of any expected trace elements [30-32], using CHN elemental analysis and XRF. Table 1 shows the weight percentage of the analyzed elements. The impurities amount to a total of 1.2 wt%, supposing that there are no other significant trace elements. We can therefore conclude that frustules of highly pure silica were obtained.

Table 1. Trace elements quantified in the cleaned diatom frustules.

Element [a]	Weight %
P	0.42
Mg	0.38
Fe	0.12
Ca	0.12

C	0.11
Cu	0.011
K	0.0099
Zn	0.0033
S	0.0030
Cl	- [b]
Mn	- [b]
N	- [b]
Total	1.2

[a] C and N were determined by CHN elemental analysis, the other elements were determined by XRF.

[b] Not detected (below detection limit).

The frustules were visualized by SEM, as shown in Figure 1. It can be observed that the individual frustules are not intact, but instead are broken down to flat or curved plate-like pieces. Although the frustules are not preserved in one piece, the typical rib-like structures and round pore 'mouths' (the so-called strutted processes) [33] can be recognized.

The *Thalassiosira pseudonana* species was chosen for its high surface area, giving it better potential for titania immobilization. Figure 2 shows the nitrogen sorption isotherm of the cleaned frustules. The BET surface area of the sample is 115 m^2/g, which is relatively high compared to other frustules. [26] The type II isotherm is indicative of a porous structure with large mesopores, which is also confirmed by TEM imaging. Figure 3 shows TEM images of the typical pore structure, which consists of near-circular pores, with a shape and size which appear to be very consistent throughout the sample (based on additional TEM images, see Figure S2 in SI). A pore size distribution determined from the left TEM image in Figure 3 gives an average pore size of 23.2 nm.

3.2 Optimization of calcination temperature and duration

After extraction, the frustules were functionalized with titania by simply adding the silica to a solution of titanyl sulfate in acidified water and subsequently evaporating the liquid. The resulting SiO_2/TiO_2 composite was then calcined in air at elevated temperature, at which titanyl sulfate decomposes to form crystalline titania. [34] The conditions were varied by using different calcination temperatures and durations, while the amount of titania precursor used in each synthesis was kept constant (0.8 g titanyl sulfate precursor per gram of silica).

XRD analysis (Figure 4) shows that the only crystalline phase present in the calcined samples is anatase. The samples calcined at 550°C and above all show the (101) reflection of the anatase phase at 25.3°. None of the samples show any reflections corresponding to rutile or brookite phases. While in bulk titania, the phase transformation from amorphous titania to anatase can already start at 350°C and a phase transition to rutile takes place at 500°C, these transition temperature are often increased for silica-immobilized titania. This is due to the lowered mobility of the titania on the silica surface. The titania nanoparticles aggregate less and remain smaller on the silica surface, compared to pure titania. [8] The transition temperatures of titania are dependent on the particle size, and can largely increase for nanoparticles, compared to bulk titania. [35] Therefore, the silica carrier effectively thermally stabilizes the titania, by limiting the nanoparticle growth. This explains that in our samples, anatase is formed at calcination temperatures of 550-650°C and no rutile phase is observed at these temperatures.

Table 2 gives an overview of some properties of the materials calcined at different conditions. The loading of titania in the materials was determined by XRF and approximates 20 wt% for all samples. The samples' photocatalytic activity was assessed in the decomposition of gaseous acetaldehyde to

carbon dioxide. To correct for the slight differences in titania loading, the activities are expressed per mg of titania and not per mg of composite. It is clear from the data that the calcination temperature of 500°C is not high enough to give good photocatalytic activity. This is in line with the fact that the XRD intensity of the anatase peak is very low for these samples (Figure 4). XRF analysis shows that the samples calcined for 3 and 6 hours still contain 0.83 and 0.37 mmol of sulfur per gram, respectively. This confirms that the titanyl sulfate precursor was not fully decomposed and converted into titania.

The highest photocatalytic activity is obtained for the sample calcined at 550°C for 3 hours, with a value of 10.4 ppm/min per mg of titania. The samples calcined at higher temperatures still show high activities (9.5 ppm/min for the samples calcined at 600°C), but the activity clearly decreases with calcination at 650°C. These differences in photocatalytic activity can be explained by two factors, namely the crystallite size and the decrease in BET surface area caused by the calcination treatment.

Table 2. Overview of characteristics of the TiO_2/SiO_2 composites calcined at different conditions.

Calcination Temperature	**Calcination duration**	**Loading of TiO_2[a]**	**Average crystallite size[b]**	**Photocatalytic activity per mg TiO_2**	**Decrease in BET surface area after calcination[c]**
(°C)	**(h)**	**(wt%)**	**(nm)**	**(ppm/min)**	**(%)**
500	3	-[d]	-[d]	0.5	3.5
500	6	-[d]	-[d]	2.6	10
550	3	18.2	12	10.4	11
550	6	21.0	17	9.3	7.8
600	3	21.9	15	9.5	19
600	6	20.8	14	9.5	32
650	3	18.7	19	8.3	22
650	6	21.8	17	6.6	29

[a] Determined by XRF.

[b] Determined by XRD using the Scherrer equation.

[c] Determined by subjecting non-functionalized frustules to the listed calcination conditions.

[d] Not determined.

The average crystallite sizes were determined using the Scherrer equation. As will be shown in section 3.4, the titania nanoparticles on these materials are inconsistent in shape, whereas the Scherrer equation assumes spherical particles. Therefore, the average crystallite sizes obtained here should not be taken as absolute values, but are rather used to observe a trend in crystallite size. We can see that the crystallite size significantly increases at 650°C. This is in line with expectations based on existing literature. It has been established that increased calcination temperatures cause an increase in anatase crystallite size, which can lead to a decrease in photocatalytic activity. [11, 36] As for the calcination time, we only see a significant difference in crystallite size for the samples calcined at 550°C. For the samples at 600°C and 650°C, the increase in temperature seems to have a more important effect than the increase of calcination duration.

Another factor which should be taken into account is the thermal stability of the frustules. It has previously been shown that calcination conditions above 550°C damage some frustules' pore structure and the BET surface area decreases due to a partial collapse of the silica structure. [30] To assess this effect for the *Thalassiosira pseudonana* frustules, the calcination conditions were repeated on non-functionalized frustules, and the BET surface areas before and after calcination were compared (Table 2). It is clear from the data that calcination at 500 and 550°C has little effect on the BET surface area (max. 11% decrease). However, the calcination conditions at 600 and 650°C do significantly decrease the BET surface area, up to 32%. This collapse of the structure, combined with an increased crystallite

size could account for the decreased photocatalytic activity at calcination temperatures of 600 and 650°C.

3.3 Optimization of titania loading

From the results in section 3.2, we found that calcination at 550°C for 3 hours gives the highest photocatalytic activity. We then investigated how the titania loading affected the activity. To achieve this, the amount of titanyl sulfate precursor used during the impregnation procedure was varied. Figure 5 shows the XRD patterns of the obtained materials. We can clearly see that the intensity of the (101) anatase reflection increases with increasing loading, suggesting that more anatase is formed at higher loadings.

Table 3. Overview of characteristics of the TiO_2/SiO_2 composites with different titania loadings.

Amount of Ti precursor used per gram of silica (g)	**Loading of TiO_2[a] (wt%)**	**Average crystallite size[b] (nm)**	**Photocatalytic activity per mg TiO_2 (ppm/min)**
0.2	6.99	-[c]	4.8
0.4	10.5	-[c]	5.1
0.8	18.2	12	10.4
1.2	25.0	15	7.5
1.6	28.9	27	6.3

[a] Determined by XRF.

[b] Determined by XRD using the Scherrer equation.

[c] Not determined.

Table 3 lists the synthesis conditions, titania loading, average crystallite size and photocatalytic activity of the samples synthesized with different precursor ratios. Despite the higher amount of anatase formed at higher titania loadings (based on the XRD patterns in Figure 5), the photocatalytic activity decreases with loadings of 25 and 29 wt%. It seems that the increase in crystal phase is compensated by an increase in crystallite size, which causes a decrease in activity. At titania loadings of 10.5 and 7 wt%, the average crystallite size could not be determined, due to the low intensity of the XRD signals. We can thus assume from the observed trend that the crystallite sizes are around 10 nm or below. However, the photocatalytic activity at these low loadings is less than that of the sample with a loading of 18.2 wt%, presumably due to a lower crystallization grade. From these data we can conclude that at a loading close to 20 wt%, the interplay between crystallization grade and crystallite size is optimal.

3.4 Further characterization of the optimized photocatalyst

From the previous results, we found that the sample calcined at 550°C for 3 hours, with a titania loading of 18.2 wt% was the optimal photocatalyst. This sample was further investigated with TEM and STEM-EDX. The first aspect that is apparent from TEM imaging, is that almost no titania particles are found outside of the frustules, so virtually all the titania was successfully grafted to the silica. This can be seen on figure S3 in the SI. Figure 6 shows the TEM images of the optimized catalyst. Image 6a gives an overview of the functionalized material. Two types of nanoparticles seem to be present on the sample, namely the ones contained inside the pores (detailed in image 6b) and the ones on the silica surface outside of the pores (detailed in image 6c). Figure 7 shows a STEM-EDX mapping of Si and Ti of the sample, confirming that the dark particles shown on the TEM images are indeed titania nanoparticles. The size of both types of nanoparticles was measured and both average to a size of 8

nm (longest axis of each particle, based on the TEM images). This indicates that both the pores and the silica platelets are effective at grafting the titania nanoparticles and limiting their growth and aggregation. This value is also of the same order of magnitude as the one obtained via the XRD patterns and the Scherrer equation (12 nm).

We compared the optimized photocatalyst to P25, which is a commercial crystalline titania powder and is widely considered as a benchmark material for photocatalysis. In the photocatalytic degradation of acetaldehyde, P25 showed an activity of 4.3 ppm/min per mg. With an activity of 10.4 ppm/min per mg, the titania grafted on the frustules is almost 2.5 times more active, which can be related to the average anatase particle size of 12 nm, compared to 29 nm for P25 (according to the Scherrer equation). This decrease in particle size increases the available surface area of the active titania phase, thus increasing the photocatalytic activity. Smaller nanoparticles are also more active because a larger fraction of the charge carriers can reach the titania surface. [37] Additionally, as can be seen on the TEM images in Figure 6, the silica surface is not fully covered with titania, and a significant amount of silica surface is available for the adsorption of acetaldehyde. It has been established in the literature that in this case, a so-called 'adsorb and shuttle' mechanism can take place. [38] This means that the targeted pollutant can be adsorbed on a silica site close to a titania particle and then migrate on to the active titania site via diffusion. According to this mechanism, the silica is not merely an inert carrier material, but actively participates in an increase in photocatalytic activity. This effect has been observed in several studies, using different types of carriers such as activated carbon, silicates and zeolites. [39-43]

3.5 Influence of humidity on the photocatalytic activity

After the optimization of the photocatalyst, the influence of the relative humidity (RH) on the photocatalytic activity was investigated. In fact, all previously mentioned photocatalytic tests were performed in dry conditions. In the literature, generally a negative effect of humidity on the photocatalytic abatement of VOCs in the gas phase is reported. [17, 44, 45] Figure 8 shows the activity of the optimized catalyst, as well as the P25 benchmark, as a function of the relative humidity. The activity of P25 gradually decreases to 42% of the initial activity at 75% RH. The titania functionalized frustules show a different behavior with a maximum at 12.5% RH followed by a decrease to 53% of the initial activity at 75% RH.

Water has a dual function in the photocatalytic abatement of VOCs. On one hand, water can form hydroxyl radicals, which are one of the active species in the oxidation process. At high amounts of adsorbed water, the formation of hydroxyl radicals is also possible through the dissociation of hydrogen peroxide. On the other hand, if too much water is present, it can form a multilayer on the titania surface, preventing acetaldehyde to access the titania hydroxyl sites (Ti-OH), thus inhibiting the decomposition reaction. [8]

Before the start of the photocatalytic experiment, the materials were UV-illuminated for 30 min. Silica is UV-transparent and the surface composition is unaltered. Titania on the other hand undergoes a surface transformation by the formation of hydrophilic Ti-OH sites. [46] From the TEM images of the composite material (Figure 6), it is clear that the silica surface is not fully covered by titania, so that a significant amount of silanol groups (Si-OH) is available to adsorb water. So, on the composite material, both Ti-OH and Si-OH sites are present. Additionally, the specific surface area of P25 is 45 m^2/g, compared to 85 m^2/g for the composite. Therefore, supposing that the water in the air is attracted to both the Ti-OH and Si-OH surface groups, the effective water concentration at the Ti-OH sites should be lower for the composite than for pure titania, at least at low RH values. At higher RH values, even

the Ti-OH groups on the composite could become saturated with water and the activity could decrease. This hypothesis could explain the maximum in photocatalytic activity at 12.5% RH for the functionalized frustules. The relative humidity of indoor air is typically around 50%. It is obvious from Figure 8 that the activity of the functionalized frustules is not optimal at these conditions. Still, at 50% RH, the activity only decreased by 14% compared to dry air, as opposed to a decrease of 45% for P25. This proves the positive effect of the frustules for applications in indoor air purification.

3.6 Extended activity study

For application in indoor air purification, the lifetime of the catalyst is an important factor. Therefore, we studied the deactivation over time of the photocatalyst by performing a longer measurement at 50% RH, represented in Figure 9. All measurements in this work were performed by three cycles of UV-illumination for 20 minutes, where the activity stabilizes in the second and third cycles (see description in the experimental section). Here, we prolonged the third UV-cycle to 47.3 hours. After 48 hours of total reaction time, the activity stays relatively stable. Some fluctuations occur in the measurement, which might be due to fluctuations of the UV-lamp intensity. The average of the acetaldehyde concentration during the abatement phases (UV light on) is shown by the gray horizontal line in Figure 9. This average value comes to 8.0 ppm/min, per mg of titania, which is only slightly lower than the 8.6 ppm/min recorded in the short measurement (Figure 8, 50% RH), which consisted of a total reaction time of one hour. We can therefore state that although the activity of the functionalized frustules is not constant over a long period of time, there is only a very slight decrease in the average activity. In conclusion, the functionalized frustules are promising photocatalysts in the purification of indoor air, according to our test reactions at 50% RH over an extended period of time.

4. Conclusions

In conclusion, we presented a straightforward method for the synthesis of titania functionalized diatom frustules. Frustules were extracted from the diatom species *Thalassiosira Pseudonana* with a high purity and high surface area. The grafting of titania was optimized and the resulting composites were tested in the decomposition of gaseous acetaldehyde. We found the highest activity for the sample with 18.2 wt% titania loading, calcined at 550°C for three hours. The titania immobilized under these conditions is 2.5 times more active than the benchmark photocatalyst P25, which can be related to a smaller particle size of the active anatase phase. This is due to a stabilization of the titania particles on the silica surface of the frustules. When tested in realistic conditions for the purification of indoor air, namely at elevated relative humidity and extended reaction time, the photocatalyst shows promising results. This type of photocatalyst would be suitable for indoor air purification systems consisting of an air circulation device and an interior surface coated with photocatalyst and irradiated with UV light. Thus, we believe that in light of a probable increase in diatom cultivation for biofuel production, the silica frustules should not be discarded as a side product, but can be valorized in technological applications such as the one investigated in this work.

Conflict of interest

The authors declare no conflicts of interests.

Acknowledgements

The authors are grateful to the Flemish government (VLAIO) for providing funding through grant number 150663. The *Thalassiosira Pseudonana* algae were kindly provided by TomAlgae. The authors thank Katrien Haustraete, Sander Clerick and Funda Aliç for performing TEM and STEM-EDX, SEM and CHN analyses, respectively, and Isabelle Ascoop for fruitful discussions. **References**

[1] C.E. Hamm, R. Merkel, O. Springer, P. Jurkojc, C. Maier, K. Prechtel, V. Smetacek, Architecture and material properties of diatom shells provide effective mechanical protection, Nature, 421 (2003) 841-843.
[2] T.V. Ramachandra, D.M. Mahapatra, B. Karthick, R. Gordon, Milking Diatoms for Sustainable Energy: Biochemical Engineering versus Gasoline-Secreting Diatom Solar Panels, Ind. Eng. Chem. Res., 48 (2009) 8769-8788.
[3] Y. Chisti, Biodiesel from microalgae, Biotechnol. Adv., 25 (2007) 294-306.
[4] M. Hildebrand, A.K. Davis, S.R. Smith, J.C. Traller, R. Abbriano, The place of diatoms in the biofuels industry, Biofuels, 3 (2012) 221-240.
[5] R.K. Iler, The Chemistry of Silica: Solubility, Polymerization, Colloid and Surface Properties and Biochemistry, Wiley, New York, 1979.
[6] E.G. Vrieling, T.P.M. Beelen, R.A. van Santen, W.W.C. Gieskes, Nanoscale uniformity of pore architecture in diatomaceous silica: A combined small and wide angle X-ray scattering study, J. Phycol., 36 (2000) 146-159.
[7] E.G. Vrieling, T.P.M. Beelen, Q.Y. Sun, S. Hazelaar, R.A. van Santen, W.W.C. Gieskes, Ultrasmall, small, and wide angle X-ray scattering analysis of diatom biosilica: interspecific differences in fractal properties, J. Mater. Chem., 14 (2004) 1970-1975.
[8] Y. Hendrix, A. Lazaro, Q. Yu, J. Brouwers, Titania-Silica Composites: A Review on the Photocatalytic Activity and Synthesis Methods, World J. Nano Sci. Eng., 5 (2015) 161-177.
[9] A.Y. Shan, T.I.M. Ghazi, S.A. Rashid, Immobilisation of titanium dioxide onto supporting materials in heterogeneous photocatalysis: A review, Appl. Catal., A, 389 (2010) 1-8.
[10] X.T. Gao, I.E. Wachs, Titania-silica as catalysts: molecular structural characteristics and physico-chemical properties, Catal. Today, 51 (1999) 233-254.
[11] D.R. Sahu, L.Y. Hong, S.C. Wang, J.L. Huang, Synthesis, analysis and characterization of ordered mesoporous TiO2/SBA-15 matrix: Effect of calcination temperature, Microporous Mesoporous Mater., 117 (2009) 640-649.
[12] Y.J. Acosta-Silva, R. Nava, V. Hernandez-Morales, S.A. Macias-Sanchez, M.L. Gomez-Herrera, B. Pawelec, Methylene blue photodegradation over titania-decorated SBA-15, Appl. Catal., B, 110 (2011) 108-117.
[13] M. Signoretto, E. Ghedini, V. Trevisan, C.L. Bianchi, M. Ongaro, G. Cruciani, TiO2-MCM-41 for the photocatalytic abatement of NOx in gas phase, Appl. Catal., B, 95 (2010) 130-136.
[14] W. Wang, M. Song, Photocatalytic activity of titania-containing mesoporous SBA-15 silica, Microporous Mesoporous Mater., 96 (2006) 255-261.
[15] A. Hanprasopwattana, T. Rieker, A.G. Sault, A.K. Datye, Morphology of titania coatings on silica gel, Catal. Lett., 45 (1997) 165-175.
[16] M.J. Lopez-Munoz, R. van Grieken, J. Aguado, J. Marugan, Role of the support on the activity of silica-supported TiO2 photocatalysts: Structure of the TiO2/SBA-15 photocatalysts, Catal. Today, 101 (2005) 307-314.
[17] M.L. Zhang, T.C. An, J.M. Fu, G.Y. Sheng, X.M. Wang, X.H. Hu, X.J. Ding, Photocatalytic degradation of mixed gaseous carbonyl compounds at low level on adsorptive TiO2/SiO2 photocatalyst using a fluidized bed reactor, Chemosphere, 64 (2006) 423-431.
[18] E. Van Eynde, T. Tytgat, M. Smits, S.W. Verbruggen, B. Hauchecorne, S. Lenaerts, Biotemplated diatom silica-titania materials for air purification, Photochem. Photobiol. Sci., 12 (2013) 690-695.
[19] J. Toster, C. Harnagea, K.S. Iyer, F. Rosei, C.L. Raston, Controlling anatase coating of diatom frustules by varying the binding layer, Crystengcomm, 14 (2012) 3446-3450.

[20] J. He, D.M. Chen, Y.L. Li, J.L. Shao, J. Xie, Y.J. Sun, Z.Y. Yan, J.Q. Wang, Diatom-templated TiO2 with enhanced photocatalytic activity: biomimetics of photonic crystals, Appl. Phys. A, 113 (2013) 327-332.
[21] W. Tang, K.H. Qiu, P.C. Zhang, X.Q. Yuan, Synthesis and photocatalytic activity of ytterbium-doped titania/diatomite composite photocatalysts, Appl. Surf. Sci., 362 (2016) 545-550.
[22] Q.Q. Zhang, R. Chen, L. Li, Synthesis of three-dimensional agaric-like biomorphic TiO2 by a facile method with Coscinodiscus sp frustule, J. Ocean Univ. China, 11 (2012) 507-510.
[23] B. Wang, F.C. de Godoi, Z.M. Sun, Q.C. Zeng, S.L. Zheng, R.L. Frost, Synthesis, characterization and activity of an immobilized photocatalyst: Natural porous diatomite supported titania nanoparticles, J. Colloid Interface Sci., 438 (2015) 204-211.
[24] L. Mao, J. Liu, S.M. Zhu, D. Zhang, Z.X. Chen, C.X. Chen, Sonochemical fabrication of mesoporous TiO2 inside diatom frustules for photocatalyst, Ultrason. Sonochem., 21 (2014) 527-534.
[25] S.K. Padmanabhan, S. Pal, E.U. Haq, A. Licciulli, Nanocrystalline TiO2-diatomite composite catalysts: Effect of crystallization on the photocatalytic degradation of rhodamine B, Appl. Catal., A, 485 (2014) 157-162.
[26] A. Gelabert, O.S. Pokrovsky, J. Schott, A. Boudou, A. Feurtet-Mazel, J. Mielczarski, E. Mielczarski, N. Mesmer-Dudons, O. Spalla, Study of diatoms/aqueous solution interface. I. Acid-base equilibria and spectroscopic observation of freshwater and marine species, Geochim. Cosmochim. Acta, 68 (2004) 4039-4058.
[27] S.O. Hay, T. Obee, Z. Luo, T. Jiang, Y.T. Meng, J.K. He, S.C. Murphy, S. Suib, The Viability of Photocatalysis for Air Purification, Molecules, 20 (2015) 1319-1356.
[28] N. Abbas, M. Hussain, N. Russo, G. Saracco, Studies on the activity and deactivation of novel optimized TiO2 nanoparticles for the abatement of VOCs, Chem. Eng. J., 175 (2011) 330-340.
[29] T. Tytgat, B. Hauchecorne, M. Smits, S.W. Verbruggen, S. Lenaerts, Concept and Validation of a Fully Automated Photocatalytic Test Setup, J. Lab. Autom., 17 (2012) 134-143.
[30] E. Van Eynde, B. Lenaerts, T. Tytgat, S.W. Verbruggen, B. Hauchecorne, R. Blust, S. Lenaerts, Effect of pretreatment and temperature on the properties of Pinnularia biosilica frustules, Rsc Advances, 4 (2014) 56200-56206.
[31] W.K. Jiang, H.Q. Pan, F.X. Wang, M.L. Jiang, X.Y. Deng, J.B. Li, A rapid sample processing method to observe diatoms via scanning electron microscopy, J. Appl. Phycol., 27 (2015) 243-248.
[32] W.K. Jiang, S.P. Luo, P.W. Liu, X.Y. Deng, Y. Jing, C.Y. Bai, J.B. Li, Purification of biosilica from living diatoms by a two-step acid cleaning and baking method, J. Appl. Phycol., 26 (2014) 1511-1518.
[33] E.E.S. Grethe R. Hasle, Karen A. Steidinger, Karl Tangen, Carmelo R. Tomas, Identifying Marine Diatoms and Dinoflagellates, Academic Press, San Diego, 1996.
[34] Y.Y. Huang, B.Y. Zhao, Y.C. Xie, A novel way to prepare silica supported sulfated titania, Appl. Catal., A, 171 (1998) 65-73.
[35] O. Khatim, M. Amamra, K. Chhor, A.M.T. Bell, D. Novikov, D. Vrel, A. Kanaev, Amorphous-anatase phase transition in single immobilized TiO2 nanoparticles, Chem. Phys. Lett., 558 (2013) 53-56.
[36] P. Cheng, M.P. Zheng, Q. Huang, Y.P. Jin, M.Y. Gu, Enhanced photoactivity of silica-titania binary oxides prepared by sol-gel method, J. Mater. Sci. Lett., 22 (2003) 1165-1168.
[37] T. Luttrell, S. Halpegamage, J.G. Tao, A. Kramer, E. Sutter, M. Batzill, Why is anatase a better photocatalyst than rutile? - Model studies on epitaxial TiO2 films, Sci. Rep., 4 (2014).
[38] Y. Paz, Composite Titanium Dioxide Photocatalysts and the "Adsorb & Shuttle" Approach: A Review, Solid State Phenom., 162 (2010) 135-162.
[39] T. Torimoto, S. Ito, S. Kuwabata, H. Yoneyama, Effects of adsorbents used as supports for titanium dioxide loading on photocatalytic degradation of propyzamide, Environ. Sci. Technol., 30 (1996) 1275-1281.
[40] N. Takeda, M. Ohtani, T. Torimoto, S. Kuwabata, H. Yoneyama, Evaluation of diffusibility of adsorbed propionaldehyde on titanium dioxide-loaded adsorbent photocatalyst films from its photodecomposition rate, J. Phys. Chem. B, 101 (1997) 2644-2649.

[41] C.H. Ao, S.C. Lee, Combination effect of activated carbon with TiO2 for the photodegradation of binary pollutants at typical indoor air level, J. Photochem. Photobiol. A: Chem., 161 (2004) 131-140.
[42] I.S. Park, S.Y. Choi, J.S. Ha, High-performance titanium dioxide photocatalyst on ordered mesoporous carbon support, Chem. Phys. Lett., 456 (2008) 198-201.
[43] R. Portela, I. Jansson, S. Suarez, M. Villarroel, B. Sanchez, P. Avila, Natural silicate-TiO2 hybrids for photocatalytic oxidation of formaldehyde in gas phase, Chem. Eng. J., 310 (2017) 560-570.
[44] A.K. Boulamanti, C.J. Philippopoulos, Photocatalytic degradation of C-5-C-7 alkanes in the gas-phase, Atmos. Environ., 43 (2009) 3168-3174.
[45] W.K. Jo, J.T. Kim, Application of visible-light photocatalysis with nitrogen-doped or unmodified titanium dioxide for control of indoor-level volatile organic compounds, J. Hazard. Mater., 164 (2009) 360-366.
[46] R. Wang, N. Sakai, A. Fujishima, T. Watanabe, K. Hashimoto, Studies of surface wettability conversion on TiO2 single-crystal surfaces, J. Phys. Chem. B, 103 (1999) 2188-2194.

Figure Captions

Figure 1. SEM images of a) the cleaned frustules, b) the pore mouths and c) the rib-like structures.

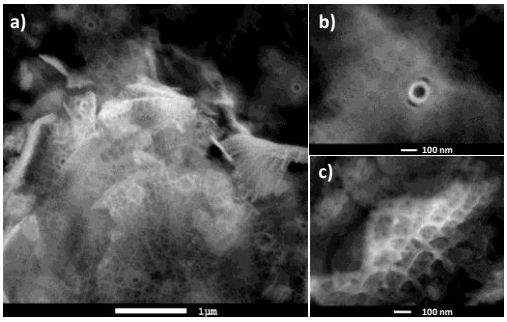

Figure 2. Nitrogen sorption isotherm of the cleaned frustules.

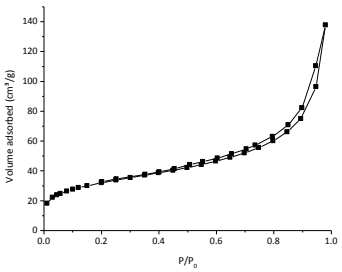

Figure 3. TEM images (a and b) of the cleaned frustules, showing the porous structure. c) shows a pore size distribution of the frustules based on image a). The distribution was based on 138 data points; the curve shows the Gaussian fit of the distribution.

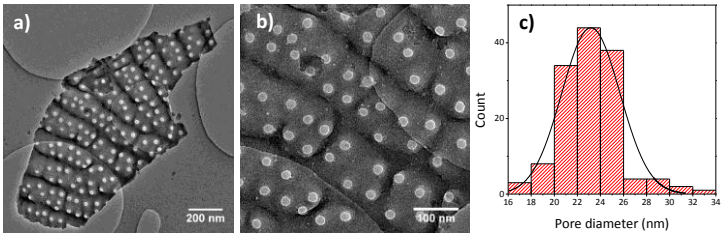

Figure 4. X-ray diffractograms of titania-functionalized frustules summarized in Table 2, calcined at different temperatures and durations. The legend indicates the calcination temperature in °C and the duration in h.

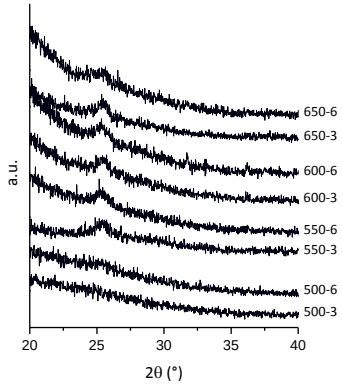

Figure 5. X-ray diffractograms of frustules functionalized with different titania loadings, summarized in Table 3. The legend indicates the Ti precursor to frustules ratio.

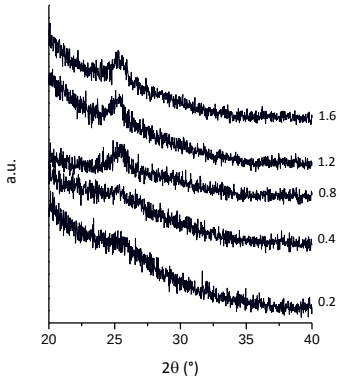

Figure 6. TEM images of the optimized titania functionalized frustules, showing an overview of the nanoparticles (a) and a detail of the nanoparticles contained inside the pores (b) and next to the pores (c).

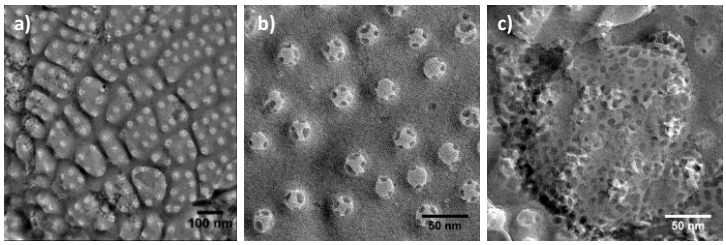

Figure 7. STEM-EDX mapping of the optimized titania functionalized frustules. Si mapping is shown in red, Ti mapping in green.

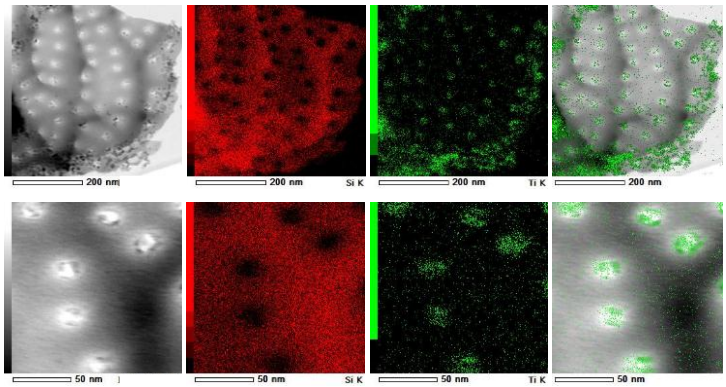

Figure 8. Photocatalytic activity of the optimized photocatalyst (●) and P25 (■) as a function of the relative humidity.

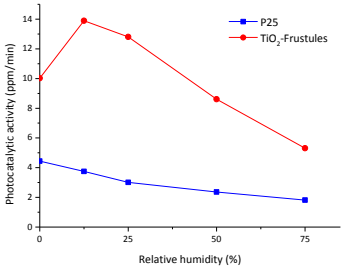

Figure 9. The concentration of acetaldehyde recorded during the photocatalytic reaction with the functionalized frustules, at 50% relative humidity. The gray line shows the average acetaldehyde concentration during the abatement phases.

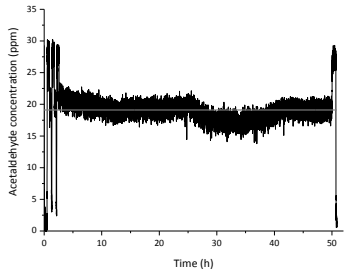

File names and desired sizing for Figures

Figure 1 – Fig1.pptx - 140 mm

Figure 2 – Fig2.pptx - 90 mm

Figure 3 – Fig3.pptx - 190 mm

Figure 4 – Fig4.pptx - 90 mm

Figure 5 – Fig5.pptx - 90 mm

Figure 6 – Fig6.pptx - 190 mm

Figure 7 – Fig7.pptx - 190 mm

Figure 8 – Fig8.pptx - 90 mm

Figure 9 – Fig9.pptx - 90 mmaa